2024 IEEE International Conference on Robotics and Automation (ICRA 2024)
May 13-17, 2024. Yokohama, Japan

An Intuitive Manual Guidance Scheme to Operate Rotation and Translation Simultaneously

Fan Shao[1] and Fanny Ficuciello[2]

***Abstract*— During certain human-robot collaboration tasks, the operator interacts with the robot by hand guidance to adjust the end-effector pose for spatial operations. The rotational operation is less intuitive to humans than translation. In fact, imagining the path to the target orientation is more challenging. In the literature related to control strategies for robot manual guidance, it is usually proposed to control translation and rotation independently. Our research explored and quantified the factors that influence operational intuition. A Virtual Fixture spatial guidance framework with intuition maintenance is proposed. This novel guidance scheme enables operators to effortlessly and simultaneously control both orientation and position in an intuitive way. High operation precision and efficiency can be achieved without interfering with the main task by exploring the null space with constraint optimization.**

***Index Terms*— hand guidance, human-robot collaboration, virtual fixture**

I. INTRODUCTION

In human-robot collaboration (HRC), humans and robots work together to achieve a shared goal [1] [2]. Operators and robots can communicate their intentions through gestures, speech, and haptic signals. For instance, a force sensor is attached to the end-effector (EE) to transmit haptic information, allowing the operator to hold the EE directly to manipulate the environment rather than relying on autonomous operation. This is particularly important for safety reasons, especially in robot-assisted surgery where most procedures require guidance from human doctors [3]. Virtual Fixture (VF) is a good option that strikes a balance between human control and autonomy [4] [5] [6] [7]. The Guidance Virtual Fixture (GVF) assists operators in moving the manipulator in the desired directions and regions, improving precision, safety and efficiency in cooperative manipulation.

A. Problem Statement

When interacting with the environment, it is important to take into account not only the position but also the orientation of the EE [8]. To illustrate, the robot assisting with drilling must ensure that the drill is close to and perpendicular to the target surface [9]. One can easily imagine the shortest translational path from the current to the target position, whereas imagining the direct rotational path is more challenging. In practical applications, the operator typically attempts multiple rotation axes to rotate the EE to the desired orientation. It is quite reasonable to separate translational and rotational motion (TRm) in hands-on cooperative control.

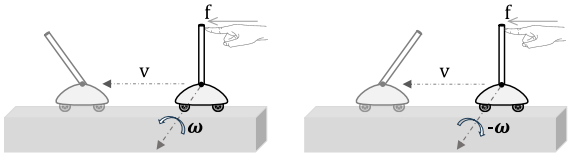

(a) Intuitive (b) Not Intuitive

Fig. 1. Intuition of TRm in manual operation

Therefore, if complicated TRm can be simplified and managed concurrently, it will be more efficient and user-friendly for manual control, especially for repetitive and energy-consuming tasks.

B. Intuition on Manual Operation

Common sense regarding motion and force states that an object moves in the direction of the force exerted on it and rotates around the torque applied. See Fig. 1(a). The goal is to move the object along the direction V and rotate the attached link around the axis ω. The desired angular motion can be achieved even if the operator only focuses on the target linear motion. Both the linear and angular motions are manipulated simultaneously and are intuitive. In Fig. 1(b), with the same target position but opposite target orientation, the operator cannot handle both at the same time. If the orientation is automatically adjusted and the operator only needs to control the translation, the rotation feedback is not intuitive. Intuitive feedback* is crucial in manual operation. It helps the operator to establish a reasonable connection between the input force and the output motion. This connection makes it easy to adjust the input force and achieve the desired goal. Without this connection, the operator is confused and unable to perform the correct operation.

The case depicted in Fig. 1(a) is specially designed for the simultaneous control of TRm. The target TRm is easy to reach and can be controlled simultaneously, even without any guidance. The case shown in Fig. 1(b) represents a more general and complex situation. It is necessary to have a human-understandable and user-friendly guidance scheme that can control the complex TRm at the same time. The method should not only increase efficiency but also provide intuitive feedback for humans.

[1]Fan Shao is with the Department of Electrical Engineering and Information Technology, University of Naples Federico II, Naples, Italy fan.shao@unina.it

[2]Fanny Ficuciello is with the Faculty of Electrical Engineering and Information Technology, University of Naples Federico II, Naples, Italy fanny.ficuciello@unina.it

*Intuitive feedback means the common sense between motion and force/torque

TABLE I
TABLUATED SUMMARY OF RESEARCH ON VF

References	Translational VF	Rotational VF	Simultaneity	Intuitive
[10] [17] [18] [11] [19] [20] [6]	✓			
[14] [15] [16] [21] [22] [23]	✓	✓		
[12] [13] [24] [25] [26] [27]	✓	✓	✓	✕
Our Method	✓	✓	✓	✓

C. Related Work

Traditional VF treats rotation and translation in $\mathbb{R}3$ space separately without considering their interrelationships in the design.

Translational guidance is well documented in the research area of HRC [10] [11]. [10] first uses admittance control to create "hard" and "soft" VFs for translatory motion. Point positioning and path following reference direction GVFs are designed to move the EE toward a set point or follow a curved path.

In some HRC scenarios, the orientation of EE also influences the application and is compensated semi-automatically without intuitive feedback when it comes to controlling translation and rotation simultaneously [12] [13]. [12] proposed a VF rule that can control the position while maintaining the orientation of EE. The authors used a stereo camera to track the surface and provide its estimated position information to generate a VF that guides EE move along the surface. Additionally, the axis orientation of EE was independently regulated to remain perpendicular to the surface or align with a preferred tool orientation. A framework for generalizing a control law for the VF rule was discussed in [13]. The Cartesian velocity controller can handle translation and rotation simultaneously. The angular motion was semi-automatically regulated and was not intuitive.

Compared to translation, orientation is less intuitive for humans. Some research focuses on manual control methods for orientation [14] [15] [16]. [14] was the first to introduce an intuitive method for representing rotational VF to facilitate the human in rotational control. Two rotational VF frameworks, the Euler vector and the rotation matrix, were introduced. Although the proposed manual guidance frameworks are human-comprehensible and can achieve low rotation error, translation and rotation are still controlled separately.

We summarized research on VF using criteria such as translational control, rotational control, simultaneity, and intuition in TABLE I. Simultaneity refers to the ability to control TRm at the same time.

D. Contribution

This paper proposes a scheme that provides the operator with helpful guidance and intuitive feedback for hands-on cooperative control.

The remainder of the paper is organized as follows: Section II describes the generation and enforcement of the intuitive VF and the variable-damping spatial guidance. Section III outlines how to quantify and maintain operational intuition. Section IV validates the accuracy and efficiency of the intuitive VF by experiments. Section V concludes the paper.

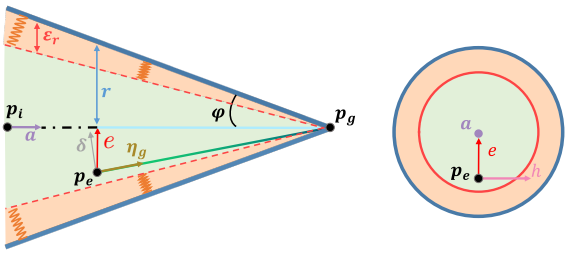

(a) Longitudinal section of VF cone (b) Cross section of VF cone

Fig. 2. Intuitive VF cone for translation

II. TRANSLATION AND ROTATION GUIDANCE

A. Virtual Fixture Generation and Enforcement

Conical VF [10] [14] can effectively assist humans in performing tasks that require high precision. A cone can be specified by its axis a and the opening angle φ as shown in Fig. 2(a), where a is a unit vector determined by the initial EE position p_i and the target position p_g, p_e is the current position, r is the cone radius.

The conical VF is used to limit the position of the EE within the cone and guide it to the target p_g. A VF guidance frame, consisting of the axes η_g, δ and h, is established to provide spatial guidance. The axes are calculated by

$$\begin{aligned} \eta_g &= \frac{p_g - p_e}{\|p_g - p_e\|}, \qquad e = (I - aa^T)(p_g - p_e), \\ \delta &= \eta_g \times (\frac{e}{\|e\|} \times \eta_g), \;\; h = \eta_g \times \delta \end{aligned} \tag{1}$$

where $I \in \mathbb{R}^{3\times3}$ is the identity matrix, e is the minimum distance from p_e to cone axis a. We chose η_g as the preferred direction, δ as the advisable direction, and h as the allowed direction if the conical constraint is not violated. If the EE moves in the preferred direction, it can reach the target position directly. The input force f_u is regulated to f_r to satisfy the conical constraint and guide the operator spatially,

$$\begin{aligned} f_{\eta_g} &= (\eta_g {\eta_g}^T) f_u, \quad f_\delta = (\delta\delta^T) f_u, \\ f_h &= (hh^T) f_u, \qquad f_r = c_p f_{\eta_g} + c_a f_\delta + c_a f_h \end{aligned} \tag{2}$$

Where c_p and c_a are scaling coefficients. The input force f_u is decomposed into f_{η_g}, f_δ and f_h along the directions of η_g, δ and h, respectively. To keep the EE moving inside the cone, any force that attempts to violate the constraint should be filtered out or reduced. If the EE position remains within the cone, the operator can move it with ease as long as he does not try to exceed the cone boundary. However, the operator will encounter resistance when trying to exceed the cone limitations. To meet these criteria, the coefficient

c_a is defined as follows:

$$c_a = \begin{cases} 0, & if\ \|e\| \geq r\ \wedge\ f \cdot \delta < 0 \\ \left[\frac{r-\|e\|}{\varepsilon_r}\right]^2, & if\ r-\varepsilon_r \leq \|e\| < r\ \wedge\ f \cdot \delta < 0 \\ 1, & others \end{cases} \quad (3)$$

The formula for calculating c_p is identical to c_a, except that only $\|e\|$ is considered in the decision criterion.

In rotational guidance, the aim is to align the current EE orientation $R^e \in \mathbb{R}^{3\times3}$ with the target orientation $R^d \in \mathbb{R}^{3\times3}$. R^e and R^d are rotation matrices with respect to the fixed base frame. $R^e_d = (R^d)^T R^e$ is the mutual orientation. To express the effect of the torque on the orientation concisely, the mutual orientation is expressed by the Euler vector o^{ed}_d, which is expressed in the desired frame, $o^{ed}_d = \theta r^{ed}_d$. Where $r^{ed}_d \in \mathbb{R}^3$ is the rotation axis, θ is the rotation angle. When EE reaches the desired orientation R^d, the Euler vector becomes the zero vector: $o^{ed}_d = (0,0,0)^T \in \mathbb{R}^3$.

The anisotropic compliance assistance method [13] is utilized to guide rotational motion. If the torque acts in the direction $-o^{ed}_d$, it drives the orientation of EE directly to R^d. So $-o^{ed}_d$ is the preferred direction of rotation. Suppose we use the control law $u = -ko^{ed}_d$ and set the angular velocity $\omega = u$. Then $\lim_{t\to\infty} R^e = R^d$. By defining the time-varying vector $g = -o^{ed}_d$, the admittance control law [28]

$$\omega = c([g] + c_\tau \langle g \rangle)\tau \quad (4)$$

can provide anisotropic rotational guidance if $c_\tau \neq 1$. Where $[g] = g(g^T g)^{-1} g^T$ is the span projection operator of g, $\langle g \rangle = I - [g]$ is the kernel of g, c controls overall compliance and c_τ the compliance of the non-preferred direction, τ is the applied torque. To ensure that EE can be easily rotated along $-o^{ed}_d$, the values $c = 0.5$ and $c_\tau = 0.2$ were chosen.

B. User Friendly Spatial Guidance

Spatial variation of the damping parameter can help the operator achieve the desired target [29]. The varying focal radius of the ellipsoid makes it a suitable representation of spatial anisotropy and allows the damping to be represented according to the direction of force. As shown in Fig. 3, the sectional view displays two half ellipsoids connected. The frame of ellipsoids is the same as the frame of VF. The right ellipsoid has the shortest semi-axis along η_g, which corresponds to the minimum damping d_{min}, while

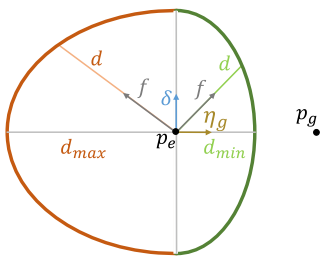

Fig. 3. Spatial anisotropy of the damping

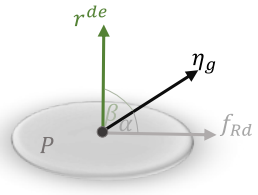

(a) Definition of β

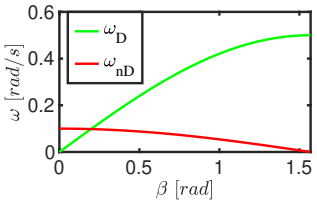

(b) The parameter β affects the operational intuition

Fig. 4. Quantitative intuition

the left ellipsoid has the longest semi-axis along $-\eta_g$, which represents the maximum damping d_{max}.

The ellipsoid-based spatial guidance is used to regulate the damping parameter for translation. The linear velocity can be determined through the admittance control law [17] [7] [2]:

$$v = \frac{f_r}{d} \quad (5)$$

The selected translational damping range is between 100 and 3000.

III. INTUITION MAINTENANCE

A. Null Space Optimization

This section explains how to maintain the intuitive control of TRm while following the VF guidance. The Intuitive Virtual Fixture (I-VF) refers to the VF guidance system that maintains intuition. In Section I-B we roughly explained the intuition of manual guidance. Manual operation is intuitive when two conditions are met. Condition 1 (COND 1): The operator can easily control the rotation and translation at the same time. Condition 2 (COND 2): The motion of EE caused by the external wrench from the operator must provide intuitive feedback to the human. The relationship between the input wrench and the translation movement is more transparent to the human than the rotational movement. The optimal manual guidance for the operator is to focus only on reaching the target position, while the angular motion caused by the input wrench simultaneously drives the EE to the target orientation and provides intuitive feedback to the operator.

Now we quantify the factors that influence intuition. Fig. 4(a) shows the rotation axis r^{de} that is extracted from R^d_e and the preferred translation direction η_g with respect to the base frame. Where β is the angle between r^{de} and η_g, P is the surface perpendicular to r^{de}. The operator can direct the EE toward the target orientation R^d by applying forces $f_R \in P$. The vector f_{Rd} coincides with the projection direction η_g on the plane P. The EE can move to the target position if the input force is along η_g. The input force along η_g can rotate EE around r^{de} only when β is 90°. And manual operation is intuitive in this way. The value of β can be selected as the intuition factor, which should be approximately 90°.

The value of β influences the simultaneity and precision of TRm, as it affects the intuition of the operation. Rewrite (4) as $\omega = \omega_D + \omega_{nD}$, where $\omega_D = c[g]\tau$ is the angular velocity

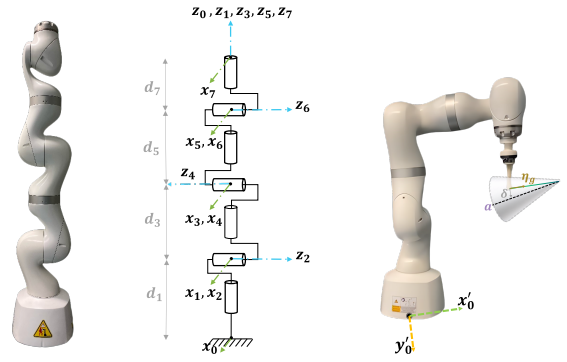

(a) Zero position (b) MDH link frames (c) Redefined base frame

Fig. 5. Link frames of the KUKA Med R800

in the preferred direction, $\omega_{nD} = cc_\tau \langle g \rangle \tau$ is the velocity in the non-preferred direction. Suppose when the operator applies a force in the direction η_g and generates a constant torque of $1\ N \cdot m$. Fig. 4(b) illustrates the relationship between ω_D, ω_{nD} and β when $c = 0.5$, $c_\tau = 0.2$. As β decreases, ω_D decreases, causing the orientation to deviate from the target. Therefore, even if the EE reaches the desired translation target, its orientation may still be far from the target. Maintaining the value of β around $90°$ ensures both intuitive operation and simultaneous control of TRm.

When β is close to $90°$, it is easy to control the translation and rotation toward the targets simultaneously, reducing the operational complexity and mental workload on the operator. Note that β is determined by current and target pose. The initial value of β can therefore be far from $90°$. In manual operation, the input force can also vary over time due to physiological tremors, causing β to change accordingly. To avoid increasing operational complexity, the β should be adjusted automatically. For the sake of consistency, we use the VF frame defined in Fig. 2 to adjust β.

We selected the KUKA LBR Med R800 robot as our research platform [30], as shown in Fig. 5(a). Its forward kinematics is

$$\dot{x} = \begin{bmatrix} v \\ \omega \end{bmatrix} = J(q)\dot{q} \tag{6}$$

where $\dot{x} \in \mathbb{R}^6$ is a vector representing the EE velocity, $\dot{q} \in \mathbb{R}^7$ is the angular velocity, and $J(q) \in \mathbb{R}^{6\times7}$ is the manipulator Jacobian. For the redundant manipulator or in the presence of redundant DOFs, a classical Inverse Kinematics (IK) solution for (6) is expressed as

$$\dot{q} = J^\dagger \dot{x} + N(q)\zeta \tag{7}$$

where $J^\dagger$ is the pseudo-inverse matrix defined by $J^\dagger = J^T(JJ^T)^{-1}$, $N(q) = I - J^T J^{\dagger T}$ is the null space projector, the vector ζ can represent the desired velocity effective in the null space after being projected by $N(q)$ into the null space of Jacobian J [2].

The optimization criteria is to increase the value of β, which is a function of the joint angle q:

$$\beta(q) = acos\left(\frac{r^{de}(q) \cdot (p_g - p_e(q))}{\|r^{de}(q)\| \|p_g - p_e(q)\|}\right) \tag{8}$$

The vector ζ can be chosen as

$$\zeta = k \nabla \beta(q) \tag{9}$$

to optimize β. Where k is the coefficient and $\nabla\beta(q)$ is the gradient of β. The gradient of β is calculated numerically. If $\beta < 90°$, k is positive, otherwise k should be negative.

β can be optimized by adjusting the position or orientation of the EE. The feedback from automatically compensated TRm will confuse the operator if the additional linear and angular motions are used to adjust β. Therefore, only the EE position p_e is automatically adjusted. Since movement in the direction η_g cannot change β, the compensation motion is only permitted in the non-preferred directions δ and h. Therefore, we can define the axes along δ and h as the null space to η_g.

When adjusting β by assigning a secondary task in the null space of the main task, the velocity $JN(q)\zeta$ should only be in the δ or h direction. The modified Denavi-Hartenberg (MDH) link frames are shown in Fig. 5(b). To satisfy the velocity constraint, the modified Jacobian $J_m \in \mathbb{R}^{6\times7}$ is defined. J_m is calculated based on the new base frame $O'_t(x'_0, y'_0, z'_0)^T$. The frame O'_t is parallel to the VF frame shown in Fig.5(c), with the x-axis (x'_0) parallel to η_g and the y-axis (y'_0) parallel to δ. The Jacobian ${J'}_m$ used in the term $N(q)$ is the 4×7 matrix that relates the joint velocity to the EE velocity along η_g, δ and h,

$$\begin{bmatrix} v_{\eta_g} \\ \omega \end{bmatrix} = {J'}_m \dot{q},\ {J'}_m = \begin{bmatrix} J_{v(1,:)} \\ J_\omega \end{bmatrix} \tag{10}$$

where v_{η_g} is the Cartesian translational velocity along η_g direction, $\omega \in \mathbb{R}^3$ is the angular velocity, $J_v \in \mathbb{R}^{3\times7}$ and $J_\omega \in \mathbb{R}^{3\times7}$ represent the linear and angular velocity components of J_m, respectively. $J_{v(1,:)}$ is the first row of J_v. The null space projector becomes $N(q) = I - ({J'}_m)^T ({J'}_m)^{\dagger T}$.

B. Integration into Constraint Optimization

The classical IK method provides an automated optimization strategy for angle β with manual guidance. However, there are two major limitations. First, as EE approaches the VF cone border, it may violate the conical constraints without introducing the velocity constraint in the null space. Second, the classical formula generally cannot optimize β close to the optimum because it only optimizes β by exploring redundancy.

The classical IK approach has an analytical solution that offers excellent computational efficiency, but it cannot handle inequality constraints. Therefore, to introduce the constraints, the general formula of IK is used [31] [32] [33]:

$$\min_{\dot{q}} \quad \frac{1}{2}\dot{q}^T Q \dot{q}, \quad s.t. \quad J\dot{q} = \dot{x} \tag{11}$$

with Q is a diagonal and positive semi-definite weighting matrix.

To incorporate the optimization of angle β into (11), an additional cost function $\beta(q)$ is included:

$$\begin{aligned} &\min_{\dot{q},q} \quad \frac{1}{2}\dot{q}^T Q \dot{q} - k\beta(q) \\ &s.t. \quad \dot{x}_{vf} - \mu B \dot{x}_{\Delta max} \le J_m \dot{q} \le \dot{x}_{vf} + \mu B \dot{x}_{\Delta max} \end{aligned} \tag{12}$$

where k is a positive coefficient multiplied by a negative sign to maximize $\beta(q)$ if $\beta < 90°$, otherwise k is negative, $\dot{x}_{vf}$ is the Cartesian velocity from VF guidance, $\dot{x}_{\Delta max} \in \mathbb{R}^6$ represents the maximum velocity $\dot{x}_\Delta$, which can be used to optimize β. It should be noted that the velocities $\dot{x}_{vf}$ and $\dot{x}_\Delta$ are relative to the newly defined base frame O'_t. The diagonal matrix $B \in \mathbb{R}^{6\times6}$ helps to select the directions of the adjustment velocity $\dot{x}_\Delta$. B is defined as $diag(\lambda_1, \lambda_2, ..., \lambda_6)$. The coefficient $\lambda_i = 1,\ or\ 0$ determines whether the adjustment velocity $\dot{x}_{i,\Delta}$ should be selected along the direction of x_i. As discussed above, the additional velocities for the optimization of β are only along δ and h to avoid influencing the movement towards the target, i.e. $\lambda_1 = 0, \lambda_4 = 0, \lambda_5 = 0, \lambda_6 = 0$. The scaling coefficient μ helps to avoid violating the cone constraint and is defined as:

$$\mu = \begin{cases} 0, & if \quad \|e\| \geq r \ \wedge \ \dot{x}_\delta < 0 \\ \left[\frac{r-\|e\|}{\epsilon}\right]^2, & if \quad r-\epsilon \leq \|e\| < r \ \wedge \ \dot{x}_\delta < 0 \\ 1, & others \end{cases} \tag{13}$$

As EE moves away from the axis, $\dot{x}_\triangle$ decreases sharply due to a reduction in μ.

The nonlinearity of $\beta(q)$ makes it difficult to solve in a fixed time. To convert (12) into a quadratic programming (QP) problem, $\beta(q)$ is linearized by Taylor polynomials:

$$\begin{aligned} \beta(q_t) &= \beta(q_{t-1}) + (\nabla\beta)^T \Delta q_t + \frac{1}{2}\Delta q_t^T H_\beta \Delta q_t \\ &= \beta(q_{t-1}) + T(\nabla\beta)^T \dot{q}_t + \frac{1}{2}T^2 \dot{q}_t^T H_\beta \dot{q}_t \end{aligned} \tag{14}$$

where H_β is the Hessian matrix of $\beta(q)$, T is the time of the control loop. Bring (14) into (12):

$$\min_{\dot{q}} \quad \frac{1}{2}\dot{q}^T Q \dot{q} - k(T(\nabla\beta)^T \dot{q}_t + \frac{1}{2}T^2 \dot{q}_t^T H_\beta \dot{q}_t) \tag{15}$$

Now arrange the parameters more compactly: $\mathcal{Q} = Q - kT^2 H_\beta$, $\mathcal{F} = -kT\nabla\beta$. The following equivalent equation can be written,

$$\begin{aligned} &\min_{\dot{q}} \quad \frac{1}{2}\dot{q}^T \mathcal{Q} \dot{q} + \mathcal{F}^T \dot{q} \\ s.t. \quad &\dot{x}_{vf} - \mu N \dot{x}_{\Delta max} \leq J_m \dot{q} \leq \dot{x}_{vf} + \mu N \dot{x}_{\Delta max} \end{aligned} \tag{16}$$

Eventually, the nonlinear optimization is transformed into a typical QP problem.

C. Sensitive Intuition Optimization

The initial value of β may not be close to 90°. If the operator attempts to guide the EE to the target, COND 1 and COND 2 will not be satisfied until β approaches 90°. The combined feedback of admittance control and optimization of β would result in the operator perceiving the robot's behavior as less transparent and unpredictable. Since the general IK method is sensitive to the gradient of β, even a small force applied to the EE, such as 0.3N, can cause the robot to react quickly to optimize β. In practice, the operator does not initially need to concentrate on moving the robot to the target, but only on maintaining gentle contact with the EE until the robot stops in the optimal state of β. The operator can then guide the robot to the target and both COND 1 and COND 2 are fulfilled.

Fig. 6. Experimental setup

IV. EXPERIMENTS

We have implemented the I-VF algorithm and tested its performance with the KUKA Med robot. The operator can interact with the robot via a handle connected to the force/torque sensor, as shown in Fig. 6.

Two experiments were conducted to evaluate the I-VF method. In the first experiment, an invisible virtual target was set. Participants were instructed to move the EE toward the target using two guidance schemes: I-VF and Separated Virtual Fixture (S-VF). S-VF refers to the separate control of translation and rotation using the VF guidance method proposed in Section II. Secondly, participants were asked to correctly position puzzle pieces on a puzzle board with geometric shapes (Fig. 6). In this experiment, the I-VF scheme was compared with the VF method and the Admittance (Adm) control with isotropic compliance.

The I-VF can provide intuitive directional feedback, allowing simultaneous manipulation of translation and orientation, while the S-VF only guides either translation or rotation at a time. Both the I-VF and S-VF methods can guide the operator to the target even without knowing its position in advance. Before the experiments, all subjects were allowed to hold the handle and manipulate the robot to gain confidence and familiarise themselves with the operation. After training, a virtual target without a visible marker was selected in the real environment. The subjects therefore did not know where the target was located. They were asked to use both I-VF and S-VF guidance in succession to move EE to the target position as quickly as possible. Fig. 7 shows the Box-plots of time, position error and orientation error for I-VF and S-VF methods. I-VF is more efficient than S-VF because

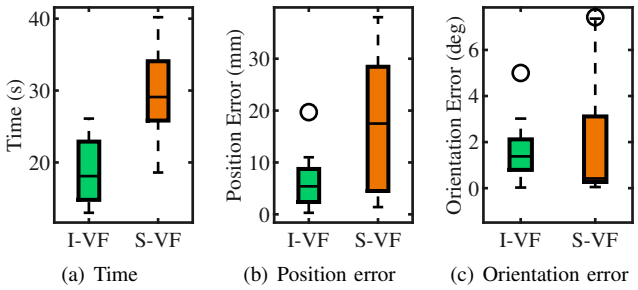

(a) Time (b) Position error (c) Orientation error

Fig. 7. Time cost and positioning precision with two different guidance schemes

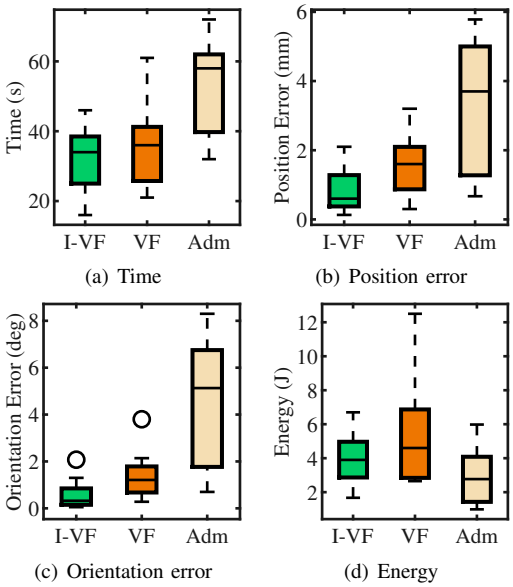

(a) Time (b) Position error (c) Orientation error (d) Energy

Fig. 8. Performances on puzzle positioning using the I-VF, VF, and Adm methods

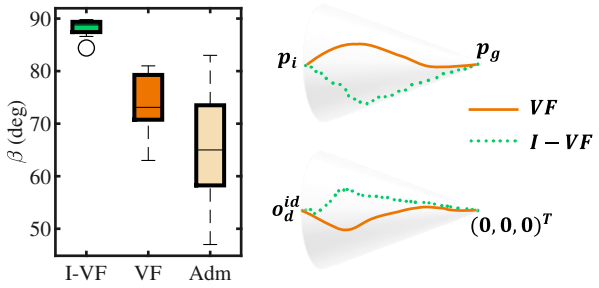

(a) Mean value of β (b) EE trajectories

Fig. 9. The values of β in I-VF, VF, and Adm. EE trajectories under the influence of β

it processes translation and rotation at once. S-VF takes 1.5 times longer than I-VF. In addition, the position and orientation accuracy of I-VF is higher and the variance is much lower than with S-VF. The significant decrease in position accuracy with S-VF is due to the separate control. After reaching the target position, the subject focused on adjusting the orientation, which would inevitably lead to a further increase in position error during the adjustment process. This experiment proves that the I-VF can be more precise and efficient by maintaining intuition.

In the second experiment, the puzzle board was secured to the desk with a bracket, and each puzzle could be attached to the EE. Before the experiment, we measured the position of the puzzle and used it as a reference target for the experiment. The initial value of β is about $54°$ and the path length is about $500 \sim 600$ mm. The I-VF method was compared with the VF and Adm methods. In the VF method, β was not automatically compensated. We chose the constant damping parameter d_{min} for the Adm method as defined in Section II-B. All volunteers must guide the robot to place a randomly selected puzzle piece in the correct position on the board using all three methods in a random sequence.

The time cost, accuracy and energy consumption statistics for I-VF, VF and Adm are displayed in Fig. 8. The time for I-VF and VF is comparable, while Adm requires more time. Since the operator can freely move the EE with Adm in an isotropic manner with constant damping, the path length could be longer than the others. The performance of Adm largely depends on the manual skills of the operator. The error variance of Adm is largest in position (3.74 mm) and rotation (7.88 deg). The damping coefficients in I-VF and VF vary depending on the input force/torque. With minimal damping, Adm requires less human effort to complete the task. I-VF also has low energy costs compared to VF.

In the experiments, β is recorded during the last 10% path of each task. It is noteworthy that the mean (88.1 deg) of β is close to $90°$ and the variance (2.96 deg) of β in I-VF is quite small, as shown in Fig. 9(a). A general case of the normalized translational and rotational EE trajectories of I-VF and VF are projected onto the longitudinal section of the cone and are shown in Fig. 9(b). In I-VF, the additional velocity used to optimize β satisfies both the velocity and geometry constraints of the cone. At the beginning of the trajectories, β is clearly and quickly optimized when the subject lightly touches the handle. After optimization, the trajectory remains close to the boundary to keep β close to $90°$. At this stage, the operator only needs to concentrate on moving the puzzle to the target position, and its orientation will simultaneously achieve the desired target. However, in VF, the trajectories stay close to the cone axis, as the resistance is greater when the EE is further away from the axis. The I-VF achieves the highest precision in translation and rotation thanks to the automatic adjustment strategy for β, with an average position error of 0.85 mm and an average rotation error of 0.63 deg.

V. CONCLUSIONS

In this paper, a VF spatial guidance framework with intuition maintenance is proposed. High operation precision can be achieved without interfering with the main task by exploring the minor or non-preferred directions as null space to optimize β with velocity and geometry constraints. In the future, we will improve the I-VF to support more complex tasks and incorporate the geometric structure of EE into the I-VF method to achieve better compatibility with different tools.

ACKNOWLEDGEMENT

The research leading to these results has been partially supported by the BRIEF "Biorobotics Research and Innovation Engineering Facilities" project (Project identification code IR0000036) funded under the National Recovery and Resilience Plan (NRRP), Mission 4 Component 2 Investment 3.1 of Italian Ministry of University and Research funded by the European Union –NextGenerationEU, partially by the LeCoR-PROC project, PRIN 2022 PNRR, identification code Prot. P20229CSJB and partially by the TI-RED project, PRIN 2022 PNRR, identification code Prot. 20229N5YW8.

REFERENCES

[1] A. Bauer, D. Wollherr, and M. Buss, "Human–robot collaboration: a survey," *International Journal of Humanoid Robotics*, vol. 5, no. 01, pp. 47–66, 2008.

[2] F. Ficuciello, L. Villani, and B. Siciliano, "Variable impedance control of redundant manipulators for intuitive human–robot physical interaction," *IEEE Transactions on Robotics*, vol. 31, no. 4, pp. 850–863, 2015.

[3] G. A. Fontanelli, L. R. Buonocore, F. Ficuciello, L. Villani, and B. Siciliano, "An external force sensing system for minimally invasive robotic surgery," *IEEE/ASME Transactions on Mechatronics*, vol. 25, no. 3, pp. 1543–1554, 2020.

[4] J. J. Abbott, P. Marayong, and A. M. Okamura, "Haptic virtual fixtures for robot-assisted manipulation," in *Robotics Research: Results of the 12th International Symposium ISRR*. Springer, 2007, pp. 49–64.

[5] S. A. Bowyer, B. L. Davies, and F. R. y Baena, "Active constraints/virtual fixtures: A survey," *IEEE Transactions on Robotics*, vol. 30, no. 1, pp. 138–157, 2013.

[6] R. Prada and S. Payandeh, "On study of design and implementation of virtual fixtures," *Virtual reality*, vol. 13, pp. 117–129, 2009.

[7] R. Moccia, C. Iacono, B. Siciliano, and F. Ficuciello, "Vision-based dynamic virtual fixtures for tools collision avoidance in robotic surgery," *IEEE Robotics and Automation Letters*, vol. 5, no. 2, pp. 1650–1655, 2020.

[8] F. Ruggiero, A. Petit, D. Serra, A. C. Satici, J. Cacace, A. Donaire, F. Ficuciello, L. R. Buonocore, G. A. Fontanelli, V. Lippiello *et al.*, "Nonprehensile manipulation of deformable objects: Achievements and perspectives from the robotic dynamic manipulation project," *IEEE Robotics & Automation Magazine*, vol. 25, no. 3, pp. 83–92, 2018.

[9] Y. Aydin, D. Sirintuna, and C. Basdogan, "Towards collaborative drilling with a cobot using admittance controller," *Transactions of the Institute of Measurement and Control*, vol. 43, no. 8, pp. 1760–1773, 2021.

[10] A. Bettini, P. Marayong, S. Lang, A. M. Okamura, and G. D. Hager, "Vision-assisted control for manipulation using virtual fixtures," *IEEE Transactions on Robotics*, vol. 20, no. 6, pp. 953–966, 2004.

[11] J. J. Abbott and A. M. Okamura, "Pseudo-admittance bilateral telemanipulation with guidance virtual fixtures," *The International Journal of Robotics Research*, vol. 26, no. 8, pp. 865–884, 2007.

[12] M. Dewan, P. Marayong, A. M. Okamura, and G. D. Hager, "Vision-based assistance for ophthalmic micro-surgery," in *Medical Image Computing and Computer-Assisted Intervention–MICCAI 2004: 7th International Conference, Saint-Malo, France, September 26-29, 2004. Proceedings, Part II 7*. Springer, 2004, pp. 49–57.

[13] G. D. Hager, "Human-machine cooperative manipulation with vision-based motion constraints," in *Visual Servoing via Advanced Numerical Methods*. Springer, 2010, pp. 55–70.

[14] D. Bazzi, F. Roveda, A. M. Zanchettin, and P. Rocco, "A unified approach for virtual fixtures and goal-driven variable admittance control in manual guidance applications," *IEEE Robotics and Automation Letters*, vol. 6, no. 4, pp. 6378–6385, 2021.

[15] A. Kapoor, M. Li, and R. H. Taylor, "Constrained control for surgical assistant robots." in *ICRA*, 2006, pp. 231–236.

[16] M. Li, M. Ishii, and R. H. Taylor, "Spatial motion constraints using virtual fixtures generated by anatomy," *IEEE Transactions on Robotics*, vol. 23, no. 1, pp. 4–19, 2007.

[17] M. Selvaggio, G. A. Fontanelli, F. Ficuciello, L. Villani, and B. Siciliano, "Passive virtual fixtures adaptation in minimally invasive robotic surgery," *IEEE Robotics and Automation Letters*, vol. 3, no. 4, pp. 3129–3136, 2018.

[18] V. Pruks, I. Farkhatdinov, and J.-H. Ryu, "Preliminary study on real-time interactive virtual fixture generation method for shared teleoperation in unstructured environments," in *Haptics: Science, Technology, and Applications: 11th International Conference, EuroHaptics 2018, Pisa, Italy, June 13-16, 2018, Proceedings, Part II 11*. Springer, 2018, pp. 648–659.

[19] Z. Jiang, Y. Liu, H. Liu, and J. Zou, "Flexible virtual fixture enhanced by vision and haptics for unstructured environment teleoperation," in *2013 IEEE International Conference on Robotics and Biomimetics (ROBIO)*. IEEE, 2013, pp. 2643–2648.

[20] T. L. Gibo, L. N. Verner, D. D. Yuh, and A. M. Okamura, "Design considerations and human-machine performance of moving virtual fixtures," in *2009 IEEE International Conference on Robotics and Automation*. IEEE, 2009, pp. 671–676.

[21] Y. Cai, P. Choi, C.-W. V. Hui, R. H. Taylor, and K. W. S. Au, "A task space virtual fixture architecture for teleoperated surgical system with slave joint limit constraints," *IEEE/ASME Transactions on Mechatronics*, vol. 27, no. 1, pp. 69–80, 2021.

[22] P. Marayong, M. Li, A. M. Okamura, and G. D. Hager, "Spatial motion constraints: Theory and demonstrations for robot guidance using virtual fixtures," in *2003 IEEE International Conference on Robotics and Automation (Cat. No. 03CH37422)*, vol. 2. IEEE, 2003, pp. 1954–1959.

[23] D. Burschka, J. J. Corso, M. Dewan, W. Lau, M. Li, H. Lin, P. Marayong, N. Ramey, G. D. Hager, B. Hoffman *et al.*, "Navigating inner space: 3-d assistance for minimally invasive surgery," *Robotics and Autonomous Systems*, vol. 52, no. 1, pp. 5–26, 2005.

[24] M. M. Marinho, H. Ishida, K. Harada, K. Deie, and M. Mitsuishi, "Virtual fixture assistance for suturing in robot-aided pediatric endoscopic surgery," *IEEE Robotics and Automation Letters*, vol. 5, no. 2, pp. 524–531, 2020.

[25] D. Zhang, Q. Zhu, J. Xiong, and L. Wang, "Dynamic virtual fixture on the euclidean group for admittance-type manipulator in deforming environments," *Biomedical engineering online*, vol. 13, pp. 1–19, 2014.

[26] R. A. Castillo-Cruces and J. Wahrburg, "Virtual fixtures with autonomous error compensation for human–robot cooperative tasks," *Robotica*, vol. 28, no. 2, pp. 267–277, 2010.

[27] M. Li, A. Kapoor, and R. H. Taylor, "A constrained optimization approach to virtual fixtures," in *2005 IEEE/RSJ International Conference on Intelligent Robots and Systems*. IEEE, 2005, pp. 1408–1413.

[28] C. Ott, R. Mukherjee, and Y. Nakamura, "Unified impedance and admittance control," in *2010 IEEE international conference on robotics and automation*. IEEE, 2010, pp. 554–561.

[29] M. H. Hamedani, M. Zekri, F. Sheikholeslam, M. Selvaggio, F. Ficuciello, and B. Siciliano, "Recurrent fuzzy wavelet neural network variable impedance control of robotic manipulators with fuzzy gain dynamic surface in an unknown varied environment," *Fuzzy Sets and Systems*, vol. 416, pp. 1–26, 2021.

[30] F. Shao and F. Ficuciello, "Dynamic parameter identification of the kuka lbr med robot," in *2023 IEEE 19th International Conference on Automation Science and Engineering (CASE)*. IEEE, 2023, pp. 1–6.

[31] K. Dufour and W. Suleiman, "On maximizing manipulability index while solving a kinematics task," *Journal of Intelligent & Robotic Systems*, vol. 100, pp. 3–13, 2020.

[32] P. Liu, D. Tateo, H. Bou-Ammar, and J. Peters, "Efficient and reactive planning for high speed robot air hockey," in *2021 IEEE/RSJ International Conference on Intelligent Robots and Systems (IROS)*. IEEE, 2021, pp. 586–593.

[33] K. Dufour and W. Suleiman, "On inverse kinematics with nonlinear criteria: Trajectory relaxation," in *2018 IEEE 15th International Workshop on Advanced Motion Control (AMC)*. IEEE, 2018, pp. 102–107.